Compressible large eddy simulations of the LP turbin TL10 cascade flow

Hitoshi FUJIWARA, Peter R VOKE& Chuichi ARAKAWA

Advanced Aircraft Research Center, NAL, JAPAN
Fluid Group, MME, UniS
The University of Tokyo

1 Abstract and Introduction

The development of the unsteady suction side boundary layer of a highly loaded LP turbine blade, TL10, has been investigated by performing compressible large eddy simulations (for TL10 cf. Schulte(1996); Schulte and Hodson(1996)). In a modern high bypass-ratio civil engine, the Reynolds number of LP turbine blade flow at design condition is very low, thus, laminar boundary layers cover most of the blade surface. In order to increase the aerodynamic load of each blade and decrease the number of blades per blade row, significant diffusion of pressure on suction surface is needed, which inevitably increases the risk of laminar separation. In order to avoid significant reduction in efficiency due to large separation, the concept of controlled boundary layer design is widely used, in which laminar separation on the suction surface is followed by transition and turbulent reattachment.

To predict the reattachment is one of the critical issues in designing LP turbine because the laminar separation without any reattachment results in large losses. However, It has been recognized that the conventional CFD using a k–ϵ turbulence model cannot predict the separation and reattachment phenomena well because these phenomena are basically unsteady. In this study, at first, the simulations with a low Reynolds number k–ϵ model were performed. After that, compressible large eddy simulations of the TL10 LP turbine flow were performed for the better prediction of the transition and reattachment on the suction surface. The results of the simulations are compared with the experimental data obtained by Schulte and Hodson(1996). Compressible Navier–Stokes equations with a low Mach number inlet condition are used for the present simulations even though the Mach number of the experimental data is so small that the flows can be treated as incompressible. One of the reasons to use the compressible equations is that the compressible simulation can be parallelized more efficiently than the incompressible counterpart because all the flow variables including pressure are solved by simple time marching integration. In other words, it is not needed to solve the Poisson equation which often causes the reduced efficiency in parallelization.

NOMENCLATURE

c_p	specific heat at constant pressure
C_p	non-dimensional blade surface pressure $(= (Pt_{\rm in} - p)/(Pt_{\rm in} - p_{out})$
c_v	specific heat at constant volume
E	total specific energy
H	total specific enthalpy $(\equiv E + p/\rho)$
L	chord length for the axial direction
M	Mach number
p	static pressure
Pr	Prandtl number
Pr_t	turbulent Prandtl number
Pt	total pressure
R	gas constant $(p = \rho RT)$
Re	Reynolds number
t	time
T	static temperature
u	velocity
x	Cartesian coordinate
ρ	density
γ	rate of the specific heats $(\equiv c_p/c_v)$
Δ	length scale of subgrid scale turbulence
Δ_g	length scale of computational grid
μ	molecular viscosity
μ_t	subgrid scale viscosity
ν	kinematic molecular viscosity $(\equiv \mu/\rho)$

SUBSCRIPTS

in	quantity at the inlet
out	quantity at the exit

2 simulation target

The simulation target is the TL10 low pressure turbine blade cascade flow(cf. Figure 1). The details of the cascade and the experimental data are provided by Schulte(1995). The Reynolds number based on the axial chode L and the exit speed U_{out} is $Re(\equiv U_{out}L/\nu) = 0.99 \sim 1.76 \times 10^5$. The Mach number of the experimental data is less than 0.01. It usually takes a long time to simulate a very low Mach number flow using Compressible Navier-Stokes equations. In order to save the computational time, a higher Mach number was assumed to save the computational time. The Mach number at the inlet was assumed to $M_{in} \simeq 0.17$, while at the exit $M_{out} \simeq 0.35$ so that the maximum Mach number of the whole flow field became less than 0.4. Compressibility effects at these Mach numbers were assumed to be negligible in this study.

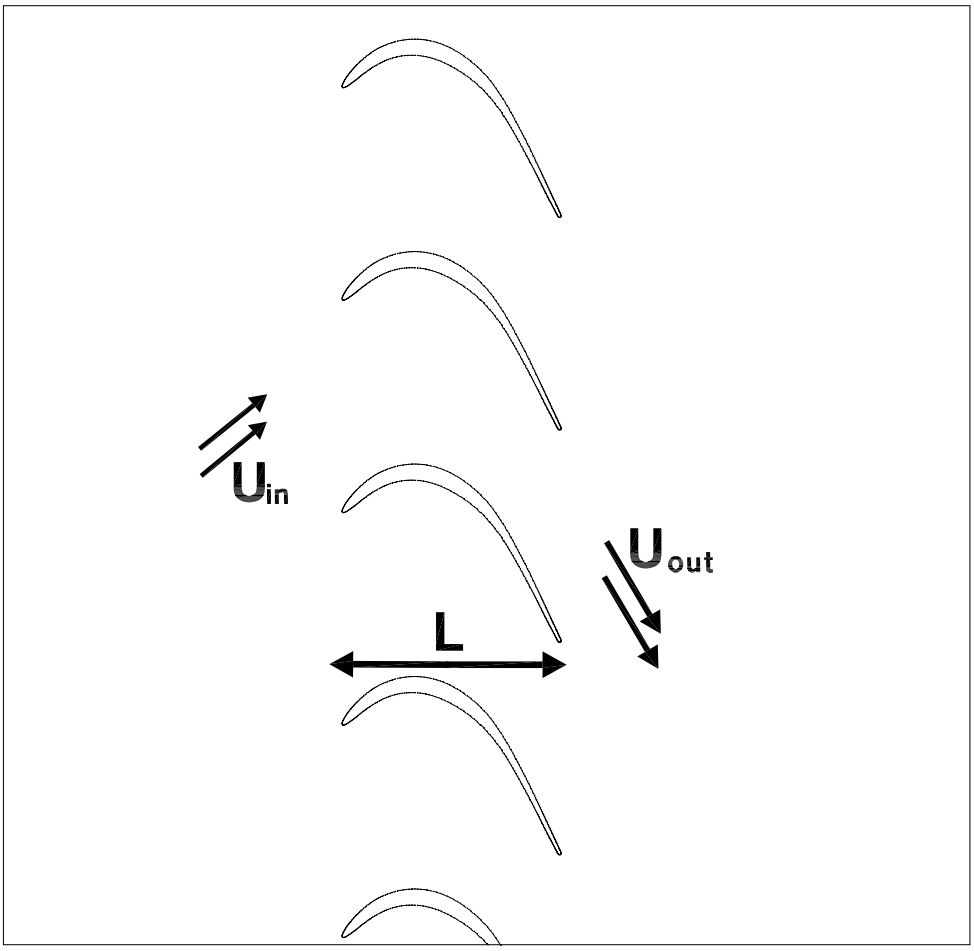

Figure 1: TL10 LP turbine cascade flow

3 Numerical methods

3.1 Governing Equations

The three–dimensional compressible Navier–Stokes equations were used for the present simulations. The equations are written by

$$\frac{\partial}{\partial t}\boldsymbol{Q} + \frac{\partial}{\partial x_j}(\boldsymbol{F}_j - \boldsymbol{G}_j) = 0 \tag{1}$$

where the conserved quantities $\boldsymbol{Q}$, the inviscid flux $\boldsymbol{F}_j$ and viscous flux $\boldsymbol{G}_j$ are given by

$$\boldsymbol{Q} = \begin{pmatrix} \rho \\ \rho\, u_i \\ \rho\, E \end{pmatrix}, \quad \boldsymbol{F}_j = \begin{pmatrix} \rho\, u_i \\ \rho\, u_i u_j + \delta_{ij} p \\ \rho\, H\, u_j \end{pmatrix}, \quad \boldsymbol{G}_j = \begin{pmatrix} 0 \\ \tau_{ij} \\ -\tau_{kj}\, u_k + q_j \end{pmatrix} \tag{2}$$

The static pressure is obtained by

$$p = (\gamma - 1)\left(\rho\, E - \frac{1}{2}\rho\, u_i^2\right) \tag{3}$$

The shear stress tensor τ_{ij} is defined by

$$\tau_{ij} = (\mu + \mu_t)\left(\frac{\partial u_i}{\partial x_j} + \frac{\partial u_j}{\partial x_i} - \frac{2}{3}\,\delta_{ij}\frac{\partial u_k}{\partial x_k}\right) \tag{4}$$

where μ_t is the Subgrid Scale(SGS) viscosity which was calculated by using Smagorinsky model(Smagorinsky 1963)

$$\mu_t = \rho(C_s\Delta)^2(2S_{ij}S_{ij})^{1/2} \tag{5}$$

$$S_{ij} \equiv \frac{1}{2}\left(\frac{\partial u_i}{\partial x_j} + \frac{\partial u_j}{\partial x_i} - \frac{2}{3}\delta_{ij}\frac{\partial u_k}{\partial x_k}\right) \tag{6}$$

with the Smagorinsky constant $C_s = 0.1$. The dumping function near the wall is given by

$$\Delta = \Delta_g[1 - \exp(\,y^+/26.0)] \tag{7}$$

The heat flux q_j is given by

$$q_j = -c_p\left(\frac{\mu}{Pr} + \frac{\mu_t}{Pr_t}\right)\frac{\partial T}{\partial x_j} \tag{8}$$

where the turbulent Prandtl number Pr_t was assumed to be 0.8.

3.2 Grid and Algorithm

The computational domain is shown in Figure 2. The width of the computation domain for the spanwise direction is equal to 40 percent of the axial chord L. H–type grids are used to resolve the whole computational region. The number of grid points is 355 for the streamwise direction, 188 for the pitchwise direction and 80 for the spanwise direction.

For time advancement, fully implicit method was used for the simulations with a k–ϵ model, while second order explicit Runge–Kutta method was used for the large eddy simulations. The results of the k–ϵ simulations were used for the initial conditions of the large eddy simulations. The time step for the large eddy simulations was equal to 0.0004 times as long as the time needed for the acoustic wave to travel for the axial chord. The convective terms, $\boldsymbol{F}_j$ on the equation (2), were evaluated using a third–order upwind biased Roe scheme(Roe 1981). The viscous terms, $\boldsymbol{G}_j$, were evaluated using a second–order central difference scheme. For the boundary conditions at the inlet, total pressure, total temperature and flow angle are fixed, while static pressure is fixed at the outlet.

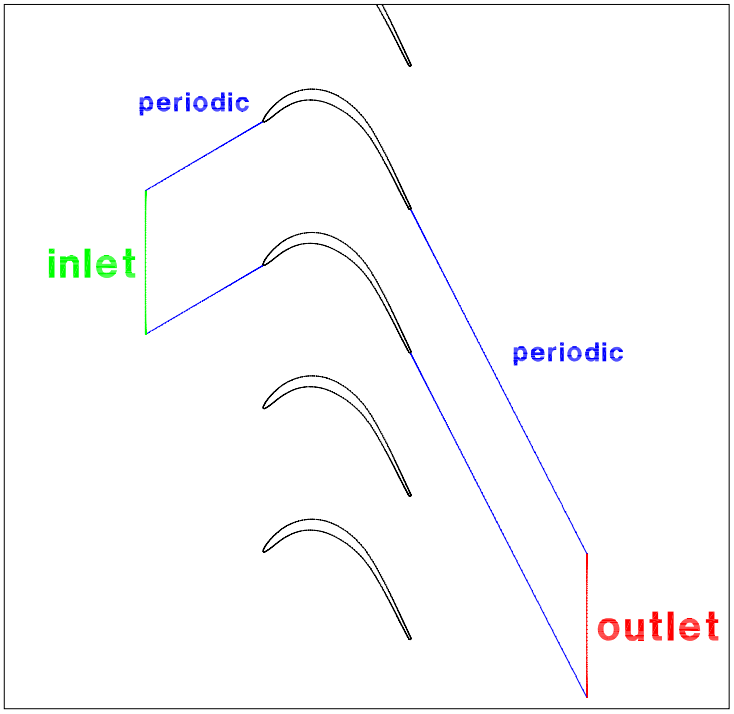

Figure 2: computational domain and boundary conditions

4 results

4.1 2D Simulations with a low Re k–ϵ model

Figure 3 compares the result of the simulation with a low Re k–ϵ model with the experimental data(Schulte and Hodson(1996)). The solid lines show the non–dimensional blade surface pressure distributions, $C_p(\equiv (Pt_{\rm in} - p)/(Pt_{\rm in} - p_{out}))$, obtained in the simulations, while the dots correspond to the experimental data. The turbulence model used was developed by Myong and Kasagi(1990). The Reynolds number based on the axial code and the exit speed is $Re = 1.3 \times 10^5$. Schulte and Hodson(1996) reported that strong diffusion on the suction surface leads to laminar boundary layer separation at about 70 percent fractional surface length point from the leading edge followed by the reattachment near the trailing edge. The rapid decrease of the measured C_p near the trailing edge on the suction surface shown in Figure 3 corresponds to the reattachment phenomena. The simulation with the k–ϵ model shows a good agreement with the experiment data on most of the blade surface, however, it does not show any decrease of C_p near the trailing edge on the suction side, which means that the simulated flow contains massive separation with no reattachment on the suction side. This disagreement is believed to be mainly caused by excessive eddy viscosity in the separated region predicted by the k–ϵ model. Another reason may be that two dimensionality and steady state are assumed in the simulation while the real flow is essentially three dimensional and unsteady near the reattachment point. Compressibility effect of the code on the resultant pressure profile seems to be a negligible problem because the overall pressure profile except near the trailing edge in the simulation agrees well with the experimental data.

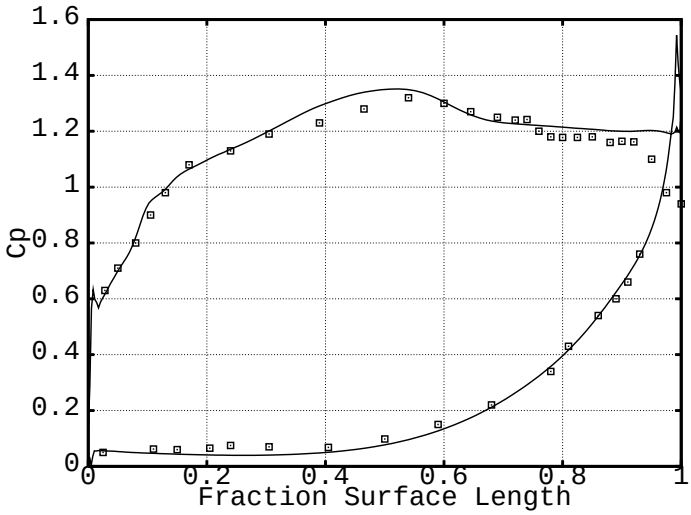

Figure 3: Blade surface pressure profile for $Re = 1.3 \times 10^5$, solid line : simulation with k–ϵ model ; points : experimental data

4.2 3D compressible large eddy simulation

Three dimensional compressible large eddy simulations of the TL10 flow were performed. The time dependent three dimensional flow fields obtained in the simulations were averaged both for time and spanwise direction. Time averaging were done for 33,000 time steps, which is long enough to obtain the stabilized data.

The solid lines in figures 4-6 show the averaged non–dimensional blade surface pressure, C_p, obtained in the large eddy simulations with the Reynolds numbers $Re = 0.99,\ 1.3,\ 1.76 \times 10^5$, respectively. Corresponding experimental data(Schulte and Hodson, 1996) are also plotted with dots. The experimental data show that reattachment occurs in all cases and that the reattachment point moves upstream on the suction surface as the Reynolds number increases. The experimental data is a reasonable one because the transition from laminar to turbulent usually occurs nearer to the separation point as the Reynolds number becomes higher, which causes earlier reattachment of the boundary layer. Figure 4 show that the C_p on the suction surface obtained in the LES slightly decreases (i.e. the surface pressure increases) near the trailing edge, which means the simulated flow field contains a symptom of reattachment. At the higher Reynolds number cases, the suction side C_p distributions obtained in the LESs show a clear reduction near the trailing edge. This means the LESs can predict the reattachment phenomena, even though the reattachment points obtained in the LESs are a little bit downstream than the experimental data. Figure 7 displays the averaged velocity field obtained in the LES with $Re = 1.76 \times 10^5$, where the reattachment after the separation can be clearly recognized.

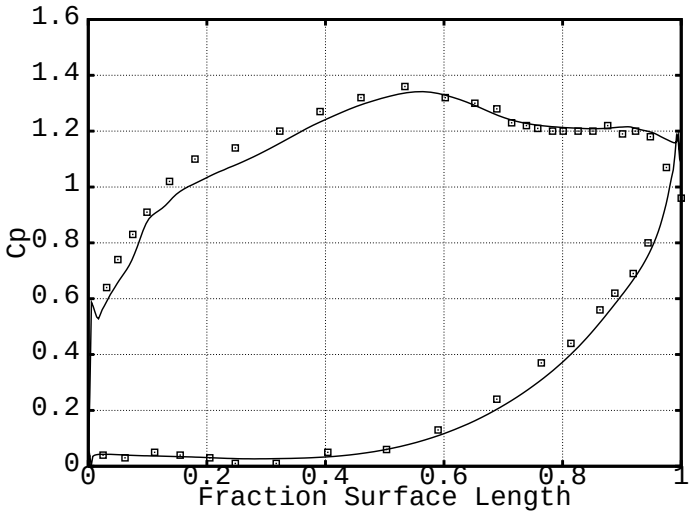

Figure 4: Blade surface pressure profile for $Re = 0.99 \times 10^5$, solid line : large eddy simulation ; points : experimental data

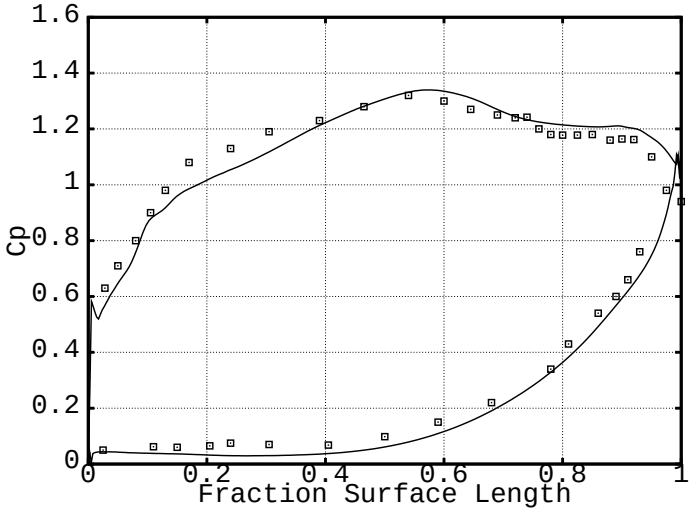

Figure 5: Blade surface pressure profile for $Re = 1.30 \times 10^5$, solid line : large eddy

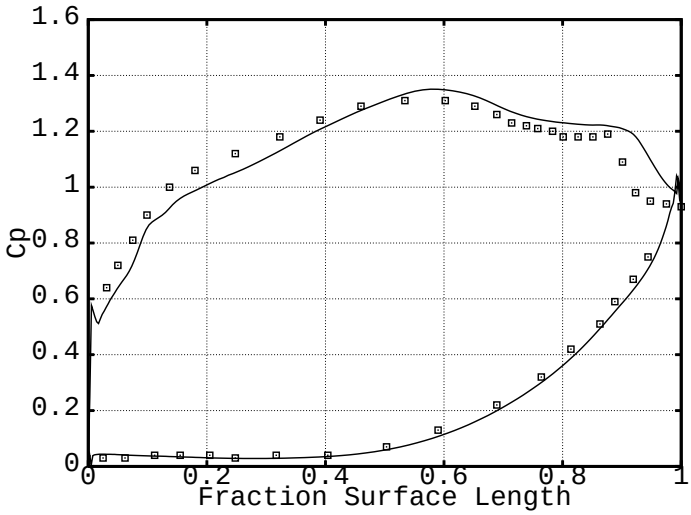

Figure 6: Blade surface pressure profile for $Re = 1.76 \times 10^5$, solid line : large eddy simulation ; points : experimental data

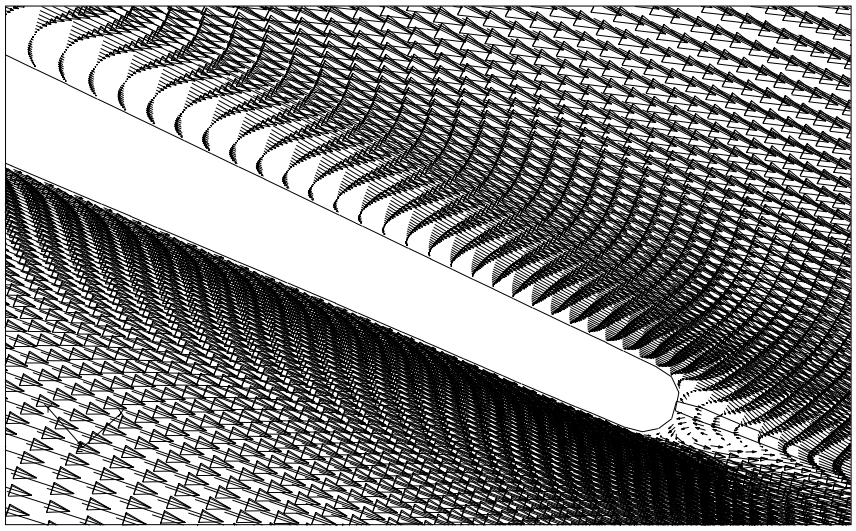

Figure 7: averaged velocity field for the LES with $Re = 1.76 \times 10^5$

In order to analyze the reattachment phenomena obtained in the large eddy simulations in detail, the three dimensional instantaneous flow field was also examined Instantaneous suction surface pressure field is shown in figure 8, which is obtained in the large eddy simulation with the Reynolds number 1.76×10^5. The figure shows that the flow is nearly two dimensional just after the separation which gradually becomes unstable and turbulent. Near the leading edge, where the flow reattaches, the simulated flow is completely three dimensional and unsteady implying that the transition from laminar to turbulence occurs. These phenomena cannot be captured by the 2D steady simulation with a k–ϵ model, which fails to predict the reattachment.

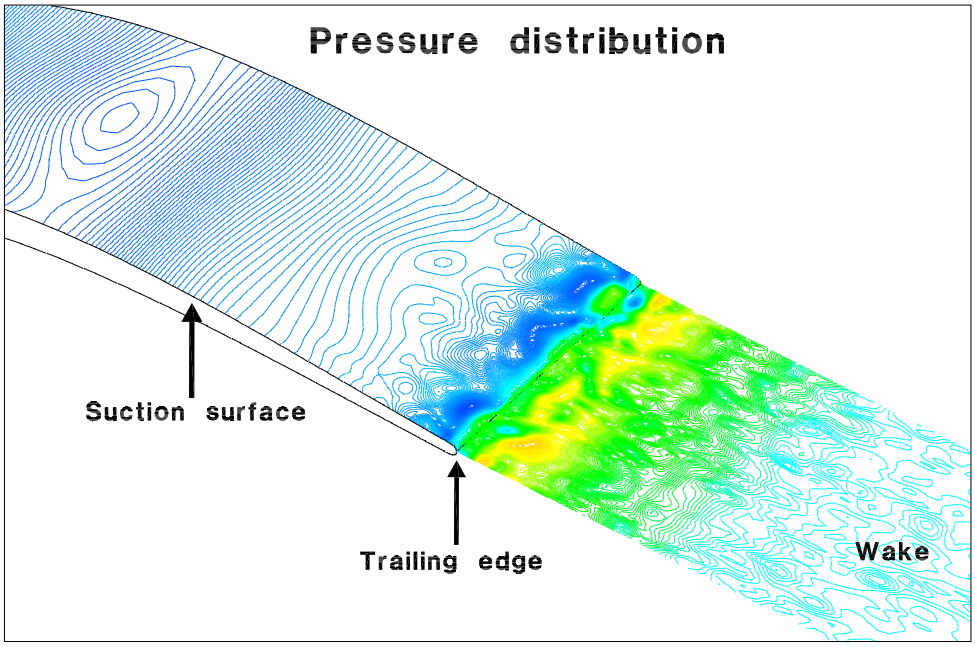

Figure 8: instantaneous suction surface pressure distribution for $Re = 1.76 \times 10^5$

5 Summary

Some of the resent results of the 3D compressible large eddy simulations of the flow through TL10 cascade with various Re number were shown. The results show that the LES can predict the boundary layer separation and reattachment process and its Re-number dependency while the 2D steady simulation with a k–ϵ model cannot. However, there is still some diversity between the LES and the experimental data on the reattachment point.

References

Schulte, V. (1995), "Unsteady separated boundary layers in axial–flow turbomachinery", Ph.D thesis, Cambride University Engineering Department. Department

Schulte, V. and Hodson, H.P. (1996), "Unsteady wake–induced boundary layer transition in high lift LP turbines", ASME 96–GT–486

Myong, H.K. and Kasagi, N. (1990), "A new approach to the improvement of k–ϵ turbulence model for wall–bounded shear flow", JSME Int. J. Fluids Eng, vol.109, 156–160.

Smagorinsky, J., (1963), Mon. Weather Rev. Vol 91, p.99.

Roe, P. L., (1981), "Approximate Rieman solvers, parameter vectors and difference schemes", J. of comp. phys. vol.43, pp.357–372.